Canonical Wnt Signaling is Involved in Anterior Regeneration of the Annelid *Aeolosoma viride*

Cheng-Yi Chen[1, †], Wei-Ting Yueh[1, †], Jiun-Hong Chen[1, *]

[1] Department of Life Science, National Taiwan University, Taipei 10617, Taiwan (R.O.C.)

[†] These authors contributed equally to the manuscript

* Correspondence should be addressed to J-H. C. (chenjh@ntu.edu.tw)

Keywords: canonical Wnt signaling, annelid regeneration, blastema proliferation and differentiation

Funding: Undergraduate Student Joining Scientific Project of National Science Council, Taiwan (NSC 97－2815－C－002－033-B).

Abstract

Annelids are regenerative animals, but the underlying mechanisms await to be discovered. Because Wnt pathway is involved in animal regeneration to varying extents, we used *Aeolosoma viride* to interrogate whether and how this pathway plays a role in annelid anterior regeneration. We found that the expression of *wnt4*, *β-catenin* and nuclear-localized β-catenin protein were up-regulated during blastemal formation and down-regulated as anterior structures gradually reformed. Consistent with potential Wnt activities in the blastema, treatments with either Wnt pathway activator (azakenpaullone) or inhibitor (XAV939) inhibited head regeneration, which further supports a role of Wnt pathway during anterior regeneration. Detailed tissue-level examines demonstrated that wound closure and blastemal cell proliferation were impaired by over-activating the pathway, and that neuronal and musculature differentiation were affected under Wnt inhibition. Combined, gene expression and chemical inhibitor data suggest the presence of dynamic Wnt activities at different anterior regeneration stages: an initial low activity may be required for wound closure, and the following activation may signal blastemal formation and cell differentiation. In a nutshell, we propose that the canonical Wnt signaling regulates blastemal cellular responses during annelid regeneration.

39

40 ## Introduction

41 Among regeneration models, researches from hydra and planarian have uncovered many
42 cellular and molecular mechanisms (King & Newmark, 2012; E. M. Tanaka & Reddien, 2011). To
43 gain more perspectives into animal regeneration and to relate to broader evolutionary
44 implications, researches in other emerging models are indispensable. Annelids are known for
45 regeneration capabilities and some underlying mechanisms are evolutionarily shared with other
46 animals. For example, similar to the neoblasts of planarian (King & Newmark, 2012; E. M.
47 Tanaka & Reddien, 2011), *Enchytraeus japonensis* and *Pristina leidyi* maintain stem cells in
48 every segment for regeneration (Myohara, 2012; Yoshida-Noro & Tochinai, 2010; Zattara,
49 Turlington, & Bely, 2016). Proliferative stem cells of planarian and *Eisenia foetida* express
50 pluripotent factors, such as *oct4*, *nanog* and *sox2* (Onal et al., 2012; Zheng, Shao, Diao, Li, &
51 Han, 2016). Consistent with the requirement of innervation for vertebrate limb regeneration
52 (Bryant, Endo, & Gardiner, 2002), diverted neuron fiber induces ectopic axis in *Eisenia* annelids
53 (Bely, 2014). However, whether any molecular mechanism regulates annelid regeneration is not
54 clear yet (Bely, 2014).

55

56 Canonical Wnt signaling pathway (i.e. the Wnt/β-catenin pathway) plays major roles in various
57 regenerative models. In hydra, injury induced apoptosis triggers the secretion of wnt3 from
58 dying cells and activates the oral pole regeneration (Chera et al., 2009). Knocking-down Wnt
59 pathway genes affect the anterior-posterior axial registration during planarian regeneration
60 (Augustin et al., 2006; Broun, Gee, Reinhardt, & Bode, 2005; Gurley, Rink, & Alvarado, 2008;

Iglesias, Gomez-Skarmeta, Saló, & Adell, 2008; King & Newmark, 2012; Lengfeld et al., 2009; Petersen & Reddien, 2008; E. Tanaka & Weidinger, 2008). Additionally, activating Wnt signaling enhances fin and limb regeneration in zebrafish and axolotl (Kawakami et al., 2006; Yokoyama, Ogino, Stoick-Cooper, Grainger, & Moon, 2007). In *Xenopus laevis,* activation of Wnt pathway rejuvenates the regenerative ability of aged limbs (Yokoyama et al., 2007). Therefore, Wnt pathway is likely to regulate regeneration in other models.

Here, we used an emerging annelid regeneration model *Aeolosoma viride* to interrogate the involvement of canonical Wnt pathway in annelid regeneration (C.-P. Chen et al., 2020). *A. viride* belongs to Aeolosomaitidae, Annelida, and is phylogenetically classified as "clitellate-like polychaetes" by morphological or molecular evidences (Hessling & Purschke, 2000; Zrzavý, Říha, Piálek, & Janouškovec, 2009). *A. viride* is a freshwater annelid, typically ranges 2-3 mm in length and 0.1-0.2 mm in width with brown spots scatter on its semitransparent epithelium. In lab conditions, *A. viride* only reproduce asexually by adding posterior segments, and the progeny detaches from the parent worm via paratomic fission (Falconi, Gugnali, & Zaccanti, 2015). Taking the advantage of its semitransparent appearance, we are able to directly observe its internal organs, such as horseshoe-shaped mouth and the digestive tract (Fig. 1A). In our preliminary tests, we found *A. viride* can robustly regenerate anterior segments in 5 days (C.-P. Chen et al., 2020). The posterior-most pygidium segment is hardly distinguishable from posterior wounds, resulting in biased assessment to successful regeneration. Therefore, we focused on anterior regeneration here.

83 In this report, we first showed transcriptional activation of *wnt4* and *β-catenin* during
84 regeneration. Then, to assay Wnt pathway activity, we labeled nuclear localized β-catenin
85 protein by immunohistochemistry. We found blastemal formation was accompanied with
86 increasing levels of nuclear β-catenin between 12-24 HPA, which was followed by dropping
87 levels of nuclear β-catenin when anterior structures gradually reformed. To functionally
88 interrogate the pathway, we treated the worms with chemical inhibitors and found that both
89 activating and inhibiting the pathway impaired regeneration. Further short-term treatments
90 demonstrated that the chemical activator blocked wound closure and blastema formation;
91 while the inhibitor affected neuron and muscle regeneration in the blastema. Lastly, we labeled
92 proliferating cells and found that cell proliferation in wound tissue was inhibited when over-
93 activating Wnt pathway. The dynamic changes of nuclear β-catenin level and discrete cellular
94 responses under inhibitor treatments suggest that wound closure, blastemal formation and cell
95 differentiation depends on mild activation of endogenous Wnt pathway. Tilting the balanced
96 pathway activity to either extremity impaired complete tissue regeneration.

97 # Results

98 **Wnt pathway is activated in the regenerating blastema**

99 To investigate whether Wnt pathway is involved in regeneration, we first tested the
100 spatiotemporal expression patterns of *wnt4, wnt8* and *β-catenin* by whole-mount *in situ*
101 hybridization (WMISH, Fig. 1). Upon amputation, the cutting plane was immediately covered by
102 *wnt4* expressing epithelial cells (Fig. 1C). Then the epithelial *wnt4* signal diminished from the
103 first hour-post-amputation (HPA) to 6 HPA before the gene was activated again at the wound
104 from 12 HPA (Fig. 1D-F). The *wnt4* signal persisted in blastema until head structures completely
105 reformed at 120 HPA (Fig. 1K). On the contrary, we did not detect significant up-regulation of
106 *wnt8* throughout the repairing process (Fig. 1M-U'), suggesting preferential Wnt ligand
107 activation during regeneration. *β-catenin* was activated from 24 HPA through 72 HPA and
108 diminished when nascent head structures became recognizable at 96 HPA (Fig. 1DD).
109
110 Additionally, we observed *wnt4* and *β-catenin* expression at the posterior 1/4th segment of
111 intact worms (Fig. 1B and V) where asexual fission occurs and EdU labeled proliferating cells are
112 enriched (C.-P. Chen et al., 2020; Falconi et al., 2015) The expression of *wnt4* and *β-catenin* at
113 this domain suggest that these genes may regulate the development of posterior growth zone,
114 like other multipotent genes, such as *piwi*, *vasa* and *nanos* in other annelids (Gazave et al., 2013;
115 Kozin & Kostyuchenko, 2015; Zheng et al., 2016).
116
117 In most studied models, active Wnt signaling cascade stabilizes cytoplasmic pool of β-catenin
118 protein, which then translocate and accumulate in the nuclei and mediate downstream gene

119 transcription (Clevers & Nusse, 2012). We labeled β-catenin protein by immunohistochemistry
120 to evaluate the pathway activity during regeneration (Fig. 2). Combining with nuclear staining,
121 we found β-catenin localized in the nuclei of regenerating blastema (Fig. 2A-D). Because
122 nascent blastema was hardly distinguishable during early wound closure, we quantified the
123 ratio of β-catenin-enriched (β-catenin$^+$) nuclei to the blastemal nuclei from 12 HPA (Fig. 2R). We
124 found that when the proliferating blastema gradually became distinguishable from wound
125 epithelium between 12 to 24 HPA, the ratio of β-catenin$^+$ nuclei increased. Then the ratio of β-
126 catenin$^+$ nuclei decreased as head regeneration completed. Combined with ISH data, we
127 proposed that Wnt signaling is activated in the proliferating blastema from 12 HPA and is
128 gradually silenced until regeneration completes at 120 HPA.
129
130 **Perturbing Wnt pathway inhibited *A. viride* regeneration**
131 We next asked whether tuning Wnt pathway can modulate *A. viride* regeneration or not. To
132 further test the role of Wnt signaling in *A. viride* regeneration, we incubated amputated worms
133 in chemical activators: Wnt Agonist, Alsterpaullone (a GSK-3β inhibitor) and 1-azakenpaullone
134 (Azkp, a GSK-3β inhibitor) or inhibitor: XAV939 (XAV, a tankyrase inhibitor and, in turn stabilizes
135 axin Broun et al., 2005; Huang et al., 2009; Kunick, Lauenroth, Leost, Meijer, & Lemcke, 2004).
136 Since endogenous Wnt pathway was activated during blastemal initiation, we expected
137 chemically activating Wnt pathway may enhance blastemal proliferation. However, to our
138 surprise, these compounds inhibited *A. viride* regeneration in dose-dependent manners (Fig.
139 3A-D). For consistency, we applied 0.25 μM Azkp or 5 μM XAV in the following experiments. We
140 found smaller blastema of Azkp treated worms, suggesting over-activating Wnt pathway may

141 inhibit blastema formation (Fig. 3H-J). On the other hand, XAV did not affect blastema
142 formation (Fig. 3K-M), but worms did not regenerate prostomium (Fig. 3G, M).
143 Additionally, we validated the inhibitor effects by assaying the nuclear β-catenin level in Azkp or
144 XAV treated blastema (Fig. 2I-R). As expected, Azkp resulted in more nuclear localized β-catenin,
145 whereas XAV treated blastema showed less nuclear β-catenin than control at 24 and 48 HPA,
146 demonstrating the efficacy of these inhibitors.
147
148 In the above assays, we applied treatments throughout regeneration and found both Wnt
149 pathway activator and inhibitor impaired regeneration. From nuclear β-catenin level of control
150 worms, we found dynamic Wnt activities during regeneration. We hypothesized that different
151 Wnt pathway activities may be required at different regeneration stages. To test the hypothesis,
152 we applied 24H pulse of Azkp or XAV for detailed temporal examinations (Fig. 3N-O). We found
153 treatments of Azkp and XAV before 72 HPA resulted in greater incidences of defective
154 regeneration, suggesting the activity of Wnt pathway is required during early regeneration
155 stages. However, the two treatments showed different effective time windows: 0-24 HPA
156 amputees were sensitive to Azkp, while 24-48 HPA amputees were sensitive to XAV. Combining
157 nuclear β-catenin data with 24H pulse treatments, we propose that wound tissue may require
158 low Wnt pathway activities during initial 0-24 HPA and then high activities between 24-48 HPA.
159
160 **Perturbing Wnt pathway impaired neuron and muscle regeneration**
161 Our key criteria for assaying anterior regeneration of *A. viride* are the reformation of head
162 structures (the prostomium, the horseshoe-shaped mouth in the peristomium, Fig. 1) and free

163 gliding behavior on substrates. Since the majority of Azkp and XAV treated amputees failed to
164 meet these criteria, we asked whether the neuron or muscle regeneration is impaired. We first
165 examined the underlying innervation by immunolabeling acetylated α-tubulin (Fig. 4). After five
166 days of regeneration, control *A. viride* recovered anterior neuron connections between the
167 neuropils and the ventral nerve cords through the circumesophageal commissures, as well as
168 dorsal-anterior sensory organs of the prostomium (Fig. 4A, D; Hessling & Purschke, 2000). Azkp
169 treated worms failed to regenerate prostomium, and the ventral nerve cords of the remaining
170 tissue showed degeneration and did not extend anteriorly to form circumesophageal
171 commissures or neuropils (Fig. 4E, H). The XAV treated worms showed partial recovery of the
172 neuron connection from the ventral nerve cords to the neuropil through the circumesophageal
173 commissures (Fig. 4I, L). However, the prostomium and the innervation from neuropil to the
174 dorsal-anterior sensory organs were missing, which may be the main reason for the failure of
175 behavioral recovery.
176
177 The rhomboid shape-arrayed muscle net underlying the intact prostomium supports its flat
178 shape and multi-directional movements (Fig. 4B). Such specialized musculature of prostomium
179 can be distinguished from the rest of body segments, which is composed by the perpendicular-
180 arrayed longitudinal and circular muscles. In addition to the observed neuronal regeneration
181 defects, both Azkp- and XAV-treated worms did not regenerate the characteristic prostomium
182 musculature (Fig. 4F, J), which further supported the observed regeneration defects from
183 morphology and behavior.
184

185 **Over-activating Wnt signaling by Azkp resulted in blastemal cell proliferation defects**

186 From our previous report, we observed that wound blastema increased in size and showed the
187 most cell proliferation between 24 and 48 HPA (Fig. 3E-G; C.-P. Chen et al., 2020). At the same
188 stages, Azkp treated wound blastema did not show comparable size change like control or XAV
189 treated worms (Fig. 3E-M). Despite Azkp and XAV treatments both inhibited anterior
190 regeneration, subtle differential cellular responses to Wnt activity perturbation may exist.
191 Because the blastema of Azkp treated wounds were smaller, we hypothesized that cell
192 proliferation can be impaired in these worms. We first examined cumulative cell proliferation
193 by 5-ethynyl-2'-deoxyuridine (EdU) pulse between 24 and 48 HPA (Fig. 5B, G, L). EdU^+ cells at
194 the blastema were less condensed in Azkp treated worms than in control and XAV, suggesting
195 that over-activating Wnt compromised blastemal cell proliferation and resulted in smaller
196 blastema. Additionally, we observed that the EdU^+ cells were ectopically enriched in the 2nd
197 segment of Azkp treated worms (Fig. 5G). From single z section images, we found the secondary
198 EdU^+ cell domain located at the anterior tip of the midgut (Fig. 5J), which was observed to
199 lesser extents in control and XAV treated worms (Fig. 5E, O-P).

200

201 Additionally, we also labeled proliferating cells at 48 HPA by anti-phospho-histone 3 antibody
202 (H3P, Fig. 5C, H, M). By quantifying the $H3P^+$ cells, we found the number of proliferating cells
203 was significantly lower in the Azkp treated blastema than control and XAV treatments (Control:
204 55±33.4; Azkp: 18.8±8.2; XAV: 59.2±30.7; *p* of Control-Azkp = 0.01; *p* of Control-XAV = 0.89; *p* of
205 Azkp-XAV = 0.001; Mann-Whitney U-test). Combining EdU and H3P assays, Azkp-induced

206 blastemal formation defects can be attributed to lacking proliferation at blastema and mis-

207 regulation of proliferating domain at the 2nd segment.

208

209 # Discussion

210 In this report, we interrogated the involvement of Wnt pathway in *A. viride* anterior
211 regeneration. Wnt pathway activities were dynamic during regeneration, with the highest
212 activity at 24 HPA when the wound blastema was actively proliferating. Long term incubation
213 with either chemical inhibitor or activator of Wnt pathway impaired regeneration. Further
214 temporal experiments suggested the requirements for the relatively low Wnt activity between
215 0-24 HPA and high activity between 24-48 HPA. Examinations of innervation, musculature and
216 cell proliferation revealed the underlying cellular responses under treatments. By integrating
217 current observations, we provide the following reasonings about how Wnt pathway is involved
218 in *A. viride* regeneration.

219

220 ***A. viride* regeneration depends on dynamic Wnt signaling activities**

221 The dynamic nuclear β-catenin levels suggest Wnt pathway activity varies through stages of *A.*
222 *viride* regeneration. Thus, long-term treatments by either Azkp or XAV may counteract against
223 endogenous Wnt activities at different stages and result in the ultimate regeneration failure.
224 Then, we further narrowed the treatment into 24H pulses. We found that the two chemical
225 inhibitors were effective before 72 HPA when normal wound tissue repaired through wound
226 closure, blastemal formation and partial differentiation stages. Immediately after amputation,
227 we observed that the wound was covered by nearby *wnt4* expressing epithelium, and then
228 *wnt4* expression was down-regulated from 1 HPA until being activated again at the blastema
229 from 12 HPA. Downregulation of *wnt4* at the wound site suggests that the wnt4-mediated Wnt
230 signaling was silenced during wound healing. Therefore, Azkp treatment at this stage may

231 counteract the Wnt inactivation as well as compromise the following blastemal cell
232 proliferations. Alternatively, over-activating Wnt pathway may override endogenous activation
233 between 12-24 HPA and turn the tissue into non-permissive conditions for regeneration. Then,
234 XAV inhibited regeneration during 24-48 HPA when the most β-catenin accumulated in the
235 nuclei. Although blastemal proliferation was not affected by XAV, the underlying innervation
236 and prostomium musculature could not completely recover. Because the appearance of neuron
237 and muscle cells are signatures of blastemal cell differentiation from nascent stem cells, we
238 propose that the endogenous Wnt activation at 24 HPA can be required for blastemal cell
239 differentiation.
240
241 Collectively, as summarized in Fig. 6, our data suggest that the progression of regeneration is
242 dependent on different Wnt activities: wound closure and initial repairing occur under low Wnt
243 activity (0-24 HPA); high Wnt activity initiates blastemal proliferation (24 HPA); blastemal
244 differentiation requires median Wnt activity (24-48 HPA); continued completion of
245 regeneration after 72 HPA is inert to exogenous Wnt activity modulators.
246
247 **Wnt signaling may not regulate anterior-posterior identity of regenerating *A. viride***
248 Wnt pathway is indispensable for defining axis during embryogenesis and regeneration of many
249 animal models (Broun et al., 2005; Chera et al., 2009; Gurley et al., 2008; Iglesias et al., 2008;
250 Leclère, Bause, Sinigaglia, Steger, & Rentzsch, 2016; Lengfeld et al., 2009; Petersen & Reddien,
251 2008; E. Tanaka & Weidinger, 2008). In planarian, activating Wnt pathway promotes posterior
252 regeneration at the anterior wound; while inhibiting the pathway induces head formation at

253 the posterior wound (Iglesias et al., 2008; Petersen & Reddien, 2008). If axial patterning of Wnt
254 pathway is evolutionarily conserved in *A. viride*, we anticipated that anterior regeneration
255 would be enhanced when we inhibited the pathway, and that posterior regeneration would be
256 enhanced when we over-activated the pathway. However, our current data and methods do
257 not support such hypothesis, i.e. XAV did not enhance anterior regeneration. Additionally, we
258 did not observe ectopic head regeneration from the posterior wounds from our preliminary
259 XAV treatments. Prostomium and anterior neuronal regeneration were inhibited by XAV
260 treatments, suggesting other side effects existed. On the other hand, anterior regeneration was
261 inhibited when the pathway was over-activated by Azkp, but we could not confidently claim
262 that these Azkp treated wounds were transformed to posterior identity for lacking axial
263 markers. Therefore, labeling anterior-posterior molecular markers will be the future direction
264 for testing whether Wnt pathway regulates the axial identity of regenerating *A. viride*.
265
266 **GSK-3β activity is required for *A. viride* neuronal regeneration and maintenance**
267 Innervation to the regenerating tissues can be necessary and sufficient for complete
268 regeneration in many systems (A. Kumar & Brockes, 2012). For example, bisected salamander
269 limbs cannot regenerate if the remaining neuron is removed (A. Kumar & Brockes, 2012);
270 ectopic neuron growth initiates ectopic blastemal formation in annelids (Bely, 2014). In
271 planarian, β-catenin-1 localizes in the nuclei of brain and ventral nerve cords and is required for
272 brain patterning during regeneration (Hill & Petersen, 2015; Sureda-Gómez, Martín-Durán, &
273 Adell, 2016). Azkp treatment results in neuronal regeneration defects in planarian, such as
274 smaller cephalic ganglia and ectopically projected visual axons (Adell, Marsal, & Saló, 2008).

275 Consistent with this idea, the Azkp treated *A. viride* did not regenerate neurons and showed
276 degenerating ventral nerve cords, suggesting the requirement of GSK-3β in neuronal
277 regeneration and maintenance. On top of that, planarian neuron regeneration is required for
278 blastemal morphogenesis (Adell et al., 2008). In *A. viride*, the blastemal cell proliferation and
279 innervation were both impaired when GSK-3β was inhibited by Azkp, suggesting a linkage
280 between neuron regeneration and blastema formation. If neuron is generally required for
281 regeneration in diverse animal models, then it is likely that *A. viride* blastema formation can be
282 also regulated by innervation, which possibly requires active GSK-3β. However, the epistatic or
283 mutual regulation of innervation and blastema formation in *A. viride* is not clear yet and
284 warrants further investigations.
285
286 In summary, we demonstrated that proper regulation of Wnt signaling activities is required for
287 different stages of *A. viride* anterior regeneration. As an echo to other regeneration models, our
288 data further generalize the involvement of Wnt signaling to regeneration in an evolutionarily
289 conserved perspective. In the future, more sophisticate approaches, such as CRISPR/Cas9
290 mutagenesis, will provide detailed molecular mechanisms of annelid regeneration as well as
291 comparative regeneration biology in a broader context.
292

293 # Materials and methods

294 **Animal husbandry**

295 Animal husbandry followed Chen et al. 2020. The whole culturing colony was asexually

296 descended from one single worm to avoid genetic differences.

297

298 **Amputation**

299 Before anterior amputation, *A. viride* was first bisected between the midgut and hindgut

300 junction (Fig. 1A). By this method, we aimed to synchronize the posterior segments and to

301 prevent any proliferating progeny interfering with assessing successful regeneration (C.-F. Chen,

302 Sung, Chen, & Chen, 2018). During synchronization, *A. viride* was cultured in ASW at 25°C

303 without feeding. The pygidium recovered in three days. Then, the anterior segments were

304 amputated between the foregut and midgut junction (Fig. 1A).

305

306 By 144 hour-post-amputation (HPA), successful anterior regeneration was assessed by the

307 following criteria: **1**) muscle contraction in prostomium and peristomium, **2**) appearance of

308 horseshoe-shaped mouth (Fig. 1A); **3**) voluntary gliding behavior on substrates. Regeneration

309 rates were assayed by averaging the proportion of successful regeneration worms form at least

310 3 biological replicates. Each replicate was started from >10 worms at 0 HPA.

311

312 **Isolation of *A. viride wnt4*, *wnt8*, and *β-catenin* sequences**

313 Total RNA of *A. viride* was purified from intact worms by TRIzol (Thermo Fisher Scientific;

314 Waltham, MA) following manufacturer's instructions. Then, the cDNA library was reverse-

315 transcribed by SuperScriptIII Reverse Transcriptase (Thermo Fisher Scientific) with oligo dT as
316 the first strand primer. Using cDNA library as template and degenerated primers (Table 1), we
317 amplified target fragments by PCR, cloned the fragments into T&A™ vector (Yeastern Biotech
318 Co., Taiwan), and sequenced the insert fragment.
319
320 For 3' Rapid Amplification of cDNA Ends (3' RACE), the cDNA library was primed by 3' end
321 anchor primer (3' AP, Table 2). Then gene specific internal primers and 3' AP head primer were
322 used for nested PCR (Table S2). The amplified products were cloned into T&A™ vector and
323 sequenced.
324
325 To amplify the 5' end sequence, we performed 5' RACE by reverse transcribing the first strand
326 cDNA by gene specific primer (Table 2). Then multiple deoxycytidines were added to the 3' end
327 of cDNA by terminal deoxynucleotidyl transferase (ThermoFisher). The gene specific primers
328 and universal 5' end anchor primer (5' AP, Table 2) were used to amplify the 5' end sequence.
329 Secondary nested PCR with 5' AP head primer (Table 2) was used to further amplify the specific
330 sequence, which is followed by cloning and sequencing as described above.
331
332 **Gene homology analysis**
333 Thirteen subfamilies of Wnt homologues proteins were previously identified in
334 Lophotrochozoan genomes (Cho, Vallès, Giani, Seaver, & Weisblat, 2010; Prud'homme, Lartillot,
335 Balavoine, Adoutte, & Vervoort, 2002). To test the homology of *A. viride wnt* genes, we first
336 used SMART protein analysis (http://smart.embl.de/) to identify the WNT domain of

337 Lophotrochozaon Wnt genes and aligned them by the default parameter of MUSCLE of MEGA7
338 program (S. Kumar, Stecher, & Tamura, 2016). Then, the phylogenetic relationship of wnts were
339 resolved by Neighbor-joining method by p-distance model with 10,000 bootstrap repeats
340 clustering *A. viride wnt4* and *wnt8* within the corresponding subfamilies (Fig. 7).
341
342 The cloned β-catenin protein encodes 12 characteristic armadillo domains (ARM) by SMART
343 analysis. The amino acid sequence of β-catenin showed higher similarity to *β-catenin* than *α-*
344 *catenin* or *γ-catenin* homologs by NCBI protein BLAST, confirming the sequence identity as *Av-*
345 *β-catenin*.
346
347 **Chemical inhibitor treatments**
348 Anterior amputated *A. viride* were washed with treatment solutions four times before
349 incubating either through whole regeneration process (Fig. 3A-D) or at 24H intervals (Fig. 3N-O).
350 1-Azakenpaulone (Azkp; MilliporeSigma, Burlington, MA), XAV939 (XAV, MilliporeSigma),
351 Alsterpaullone (MilliporeSigma), Wnt Agonist (MilliporeSigma) were dissolved in dimethyl
352 sulfoxide (DMSO) as stock solutions, and then diluted in artificial spring water (ASW) as working
353 solutions at designed concentrations. Control solution was prepared with comparable
354 concentrations of DMSO in ASW.
355
356 **Whole-mount Immunofluorescence (WMIF)**
357 Worms were anesthetized by menthol saturated ASW, and then fixed with 4% PFA-ASW
358 overnight at 4°C. Then the samples were washed 5 times with phosphate buffered saline (PBS,

359 pH=7.4) containing 0.1% Triton X-100 (PBST). After washing, the fixed worms were rinsed with
360 100% methanol 3 times at RT and stored at -20°C until proceeded to immunohistochemistry.
361
362 To begin immunohistochemistry, the samples were re-hydrated through series of 66% and 33%
363 methanol in PBST washes and additional washes in PBST for 5 times. Then, the samples were
364 treated with 5 µg/mL protease K solution at RT for 5 minutes, followed by incubation in 2
365 mg/mL glycine for 5 minutes and post-fixation with 4% PFA-PBST at RT for 1 hour. After post-
366 fixation, the samples were washed 3 times with PBST, and immersed in the blocking solution
367 (PBST with 3% bovine serum albumin and 5% Goat serum) for up to 1 hour at RT. Primary
368 antibody incubation: Rabbit-anti-β-catenin antibody (in 1:800 dilution; MilliporeSigma, C2206),
369 Rabbit-anti-H3P antibody (in 1:1000 dilution; MilliporeSigma, 06-570) or Mouse-anti-acetylated
370 α-tubulin (in 1:1000 dilution; MilliporeSigma, T7451) was applied overnight at 4°C with blocking
371 solution as diluent. After 6 times washing with PBST, samples were incubated in fluorophore
372 conjugated Goat anti-Rabbit antibody or Goat anti-Mouse antibody (in 1:400 dilution; Thermo
373 Fisher Scientific) for 2 hours at RT with blocking solution as diluent. F-Actin staining was
374 performed on no methanol treated samples as follows: After 1 hour blocking by 1% BSA-PBST at
375 RT, we incubated samples in BODIPY® FL Phallacidin (1:40 dilution in blocking buffer, Thermo
376 Fisher Scientific) at RT for 1 hour. The nuclei were counter-stained with 1 µg/mL DAPI-PBST for
377 20 minutes at RT. After 4 times washes by PBST, the samples were immersed and cleared in
378 80% glycerol-PBS with 0.1% NaN_3 before mounting on slides.
379
380 **Whole-mount *in situ* hybridization (WMISH)**

381 DNA templates of riboprobes were amplified by gene specific primers (Table 3) and cloned into
382 T&A^{TM} vector. After confirming the desired orientations by sequencing, we linearized the
383 plasmids as templates for DIG-labeled riboprobes synthesis by T7 polymerase (Thermo Fisher
384 Scientific) with DIG RNA labeling mix (MilliporeSigma).
385
386 The WMISH protocol was adopted from zebrafish WMISH protocol (Thisse & Thisse, 2008).
387 Sample preparation was similar to WMIF, but PBS with 0.1% Tween-20 (PBSTw) was used
388 instead of PBST. Pre-hybridization was performed in HYB$^-$ buffer (50% formamide, 5X SSC, and
389 0.1% Tween-20 in DEPC-treated H_2O) at 65 °C for 1 hour. The riboprobes were diluted at 1
390 ng/µL in HYB$^+$ buffer (HYB$^-$ buffer with 50 µg/mL Heparin and 0.5 mg/µL yeast tRNA;
391 MilliporeSigma). Hybridization was performed at 65 °C overnight. Then samples were washed at
392 65 °C by serial dilutions of HYB$^-$ and 2X SSCTw (2X SSC with 0.1% Tween-20) from 2:1 to 1:2 ratio,
393 one 2X SSCTw wash, two 0.2X SSCTw (0.2X SSC with 0.1% Tween-20) washes, and another serial
394 dilution of 0.2X SSCTw and PBSTw from 2:1 to 1:2 ratio. The samples were washed once by
395 PBSTw at RT and immersed in blocking solution (5% BSA in PBSTw) at 4 °C overnight. The
396 samples were then incubated in 1:10,000 diluted anti-DIG-AP antibody (MilliporeSigma) in
397 blocking buffer at 4 °C overnight. Then samples were washed 10 times with PBSTw and 3 times
398 with AP buffer (0.1 M Tris-Cl, 0.05 M $MgCl_2$, 0.1 M NaCl and 0.1% Tween-20 in DEPC-treated
399 H_2O). NBT and BCIP were added in AP buffer for colorimetric reaction at 4 °C overnight. Finally,
400 the reaction was stopped by 5 times PBSTw washes and once 100% methanol wash before
401 immersing in 80% glycerol-PBS for mounting.
402

403 **EdU labeling**

404 Regenerating *A. viride* were incubated in 100 µM 5-ethynyl-2'-deoxyuridine (EdU; Thermo
405 Fisher Scientific) diluted in ASW from 24 to 48 HPA, when blastemal cells showed the most
406 proliferation (C.-P. Chen et al., 2020). Then, worms were anesthetized and fixed as WMIF
407 method. After protease K treatment and re-fixation, Click-iT® reaction was performed as
408 manufacturer's instruction (Click-iT® EdU Imaging Kits, Thermo Fisher Scientific). Experiments
409 validated the specificity of EdU is shown in Fig. 8.

410

411 **Microscopy**

412 Images of regenerating worms and *in situ* hybridization were taken by Stereo Investigator (MBF
413 Bioscience), Zeiss Axio Observer Z1 or Zeiss Axio Imager A1 microscope with a Zeiss AxioCam
414 MRc CCD camera. Fluorescent specimens were imaged by Leica TCS SP5 confocal laser scanning
415 microscope. Contrasts of images were adjusted as the corresponding control images by ImageJ.
416 Figures were prepared by Illustrator CC (Adobe).

417

418 **Image quantification**

419 β-catenin$^+$ and H3P$^+$ nuclei were manually quantified through z-stacks of regenerating blastema
420 by Fiji: in brief, the images were pre-processed by "Subtract Background", "Median" and the
421 nuclei were quantified by "3D Maxima Finder" (Boudier et al., 2013). EdU$^+$ nuclei quantification
422 was performed according to Cai et. al, 2009 with minor modifications (Cai, Vallis, & Reilly, 2009):
423 analysis of particles was set > 12 µm^2 corresponding to the cell size and covered the entire z
424 stack range of images.

425

426 **Statistic analysis**

427 Difference of successful regeneration rates were tested by Cochran Q test and McNemar

428 change test. The ratio of β-catenin^{+} nuclei was analyzed by two-tailed *t*-test, assuming equal

429 variances. Parametric unpaired *t*-test between treatments was performed for comparing the

430 ratio of EdU^{+} nuclei in blastema to 2nd segment with log-transformation. The number of H3P^{+}

431 nuclei in the blastema was assayed by Mann-Whitney U-test. *p* values less than 0.05 were

432 considered statistically significant.

433

434 Declarations

435 **Ethics approval and consent to participate**

436 All experimental treatments on *A. viride* were approved by the Environmental Protection and

437 Occupational Safety and Health Center, National Taiwan University.

438

439 **Availability of data and material**

440 All data generated or analyzed during this study are included in this published article, or

441 available upon reasonable request from the corresponding author.

442

443 **Competing interests**

444 The authors declare that they have no competing interests

445

446 **Authors' contributions**

447 CYC, WTY and JHC prepared the manuscript. CYC and WTY design and perform the experiments
448 and analyzed the data. All authors read and approved the final manuscript.
449

450 **Acknowledgements**
451 We would like to thank Dr. Eric Hill from Stowers Institute for Medical Research, Kansas City,
452 MO for suggestions and critics on the manuscript. We appreciate Dr. Jr-Kai Yu from Institute of
453 Cellular and Organismic Biology, Academia Sinica, Taiwan, for kindly providing access to the
454 confocal microscopy.
455

456

457 ## References

458 Adell, T., Marsal, M., & Saló, E. (2008). Planarian GSK3s are involved in neural regeneration.
459 *Development Genes and Evolution*, *218*(1–2), 89–103. https://doi.org/10.1007/s00427-
460 007-0199-3

461 Augustin, R., Franke, A., Khalturin, K., Kiko, R., Siebert, S., Hemmrich, G., & Bosch, T. C. G. (2006).
462 Dickkopf related genes are components of the positional value gradient in Hydra.
463 *Developmental Biology*, *296*(1), 62–70. https://doi.org/10.1016/j.ydbio.2006.04.003

464 Bely, A. E. (2014). Early events in annelid regeneration: a cellular perspective. *Integrative and*
465 *Comparative Biology*, *54*(4), 688–699. https://doi.org/10.1093/icb/icu109

466 Boudier, T., Ollion, J., Cochennec, J., Escude, C., Curie, M., Umr, C., … Paris, C. (2013). TANGO : a
467 generic tool for high-throughput 3D image analysis for studying nuclear organization.
468 *Bioinformatics*, *29*(14), 1840–1841. https://doi.org/10.1093/bioinformatics/btt276

469 Broun, M., Gee, L., Reinhardt, B., & Bode, H. R. (2005). Formation of the head organizer in hydra
470 involves the canonical Wnt pathway. *Development*, *132*(12), 2907–2916.
471 https://doi.org/10.1242/dev.01848

472 Bryant, S. V, Endo, T., & Gardiner, D. M. (2002). Vertebrate limb regeneration and the origin of
473 limb stem cells. *The International Journal of Developmental Biology*, *46*(7), 887–896.

474 Cai, Z., Vallis, K. A., & Reilly, R. M. (2009). Computational analysis of the number, area and
475 density of gamma-H2AX foci in breast cancer cells exposed to (111)In-DTPA-hEGF or
476 gamma-rays using Image-J software. *International Journal of Radiation Biology*, *85*(3), 262–
477 271. https://doi.org/10.1080/09553000902748757

478 Chen, C.-F., Sung, T.-L., Chen, L.-Y., & Chen, J.-H. (2018). Telomere maintenance during anterior
479 regeneration and aging in the freshwater annelid Aeolosoma viride. *Scientific Reports*, *8*(1),
480 18078. https://doi.org/10.1038/s41598-018-36396-y
481 Chen, C.-P., Fok, S. K.-W., Hsieh, Y.-W., Chen, C.-Y., Hsu, F.-M., Chang, Y.-H., & Chen, J.-H. (2020).
482 General characterization of regeneration in Aeolosoma viride (Annelida, Aeolosomatidae).
483 *Invertebrate Biology*, e12277. https://doi.org/10.1111/ivb.12277
484 Chera, S., Ghila, L., Dobretz, K., Wenger, Y., Bauer, C., Buzgariu, W., … Galliot, B. (2009).
485 Apoptotic cells provide an unexpected source of Wnt3 signaling to drive hydra head
486 regeneration. *Developmental Cell*, *17*(2), 279–289.
487 https://doi.org/10.1016/j.devcel.2009.07.014
488 Cho, S.-J. J., Vallès, Y., Giani, V. C., Seaver, E. C., & Weisblat, D. A. (2010). Evolutionary Dynamics
489 of the wnt Gene Family: A Lophotrochozoan Perspective. *Molecular Biology and Evolution*,
490 *27*(7), 1645–1658. https://doi.org/10.1093/molbev/msq052
491 Clevers, H., & Nusse, R. (2012). Wnt/β-catenin signaling and disease. *Cell*, *149*(6), 1192–1205.
492 https://doi.org/10.1016/j.cell.2012.05.012
493 Falconi, R., Gugnali, A., & Zaccanti, F. (2015). Quantitative observations on asexual reproduction
494 of Aeolosoma viride (Annelida, Aphanoneura). *Invertebrate Biology*, *134*(2), 151–161.
495 https://doi.org/10.1111/ivb.12087
496 Gazave, E., Béhague, J., Laplane, L., Guillou, A., Préau, L., Demilly, A., … Vervoort, M. (2013).
497 Posterior elongation in the annelid Platynereis dumerilii involves stem cells molecularly
498 related to primordial germ cells. *Developmental Biology*, *382*(1), 246–267.

499 Gurley, K., Rink, J., & Alvarado, A. (2008). Beta-catenin defines head versus tail identity during
500 planarian regeneration and homeostasis. *Science*, *319*(5861), 323–327.
501 https://doi.org/10.1126/science.1150029
502 Hessling, R., & Purschke, G. (2000). Immunohistochemical (cLSM) and ultrastructural analysis of
503 the central nervous system and sense organs in Aeolosoma hemprichi (Annelida,
504 Aeolosomatidae). *Zoomorphology*, *120*(2), 65–78. https://doi.org/10.1007/s004350000022
505 Hill, E. M., & Petersen, C. P. (2015). Wnt/Notum spatial feedback inhibition controls neoblast
506 differentiation to regulate reversible growth of the planarian brain. *Development*, *142*(24),
507 4217–4229. https://doi.org/10.1242/dev.123612
508 Huang, S.-M. A., Mishina, Y. M., Liu, S., Cheung, A., Stegmeier, F., Michaud, G. A., … Cong, F.
509 (2009). Tankyrase inhibition stabilizes axin and antagonizes Wnt signalling. *Nature*,
510 *461*(7264), 614. https://doi.org/10.1038/nature08356
511 Iglesias, M., Gomez-Skarmeta, J. L., Saló, E., & Adell, T. (2008). Silencing of Smed-betacatenin1
512 generates radial-like hypercephalized planarians. *Development*, *135*(7), 1215–1221.
513 https://doi.org/10.1242/dev.020289
514 Kawakami, Y., Esteban, C. R., Raya, M., Kawakami, H., Martí, M., Dubova, I., & Belmonte, J. C. I.
515 (2006). Wnt/beta-catenin signaling regulates vertebrate limb regeneration. *Genes Dev*,
516 *20*(23), 3232–3237. https://doi.org/10.1101/gad.1475106
517 King, R., & Newmark, P. (2012). The cell biology of regeneration. *Journal of Cell Biology*, *196*(5),
518 553–562. https://doi.org/10.1083/jcb.201105099

519 Kozin, V. V, & Kostyuchenko, R. P. (2015). Vasa, PL10, and Piwi gene expression during caudal
520 regeneration of the polychaete annelid Alitta virens. *Development Genes and Evolution*,
521 *225*(3), 129–138. https://doi.org/10.1007/s00427-015-0496-1
522 Kumar, A., & Brockes, J. P. (2012). Nerve dependence in tissue, organ, and appendage
523 regeneration. *Trends in Neurosciences*, *35*(11), 691–699.
524 https://doi.org/10.1016/j.tins.2012.08.003
525 Kumar, S., Stecher, G., & Tamura, K. (2016). MEGA7: Molecular Evolutionary Genetics Analysis
526 Version 7.0 for Bigger Datasets., *33*(7), 1870–1874.
527 https://doi.org/10.1093/molbev/msw054
528 Kunick, C., Lauenroth, K., Leost, M., Meijer, L., & Lemcke, T. (2004). 1-Azakenpaullone is a
529 selective inhibitor of glycogen synthase kinase-3. *Bioorganic & Medicinal Chemistry Letters*,
530 *14*(2), 413–416.
531 Leclère, L., Bause, M., Sinigaglia, C., Steger, J., & Rentzsch, F. (2016). Development of the aboral
532 domain in Nematostella requires β-catenin and the opposing activities of Six3/6 and
533 Frizzled5/8. *Development*, *143*(10), 1766–1777. https://doi.org/10.1242/dev.120931
534 Lengfeld, T., Watanabe, H., Simakov, O., Lindgens, D., Gee, L., Law, L., … Holstein, T. W. (2009).
535 Multiple Wnts are involved in Hydra organizer formation and regeneration. *Developmental*
536 *Biology*, *330*(1), 186–199. https://doi.org/10.1016/j.ydbio.2009.02.004
537 Myohara, M. (2012). What role do annelid neoblasts play? A comparison of the regeneration
538 patterns in a neoblast-bearing and a neoblast-lacking enchytraeid oligochaete. *PLoS One*,
539 *7*(5), e37319. https://doi.org/10.1371/journal.pone.0037319

540 Onal, P., Grün, D., Adamidi, C., Rybak, A., Solana, J., Mastrobuoni, G., … Rajewsky, N. (2012).
541 Gene expression of pluripotency determinants is conserved between mammalian and
542 planarian stem cells., *31*(12), 2755–2769. https://doi.org/10.1038/emboj.2012.110
543 Petersen, C. P., & Reddien, P. W. (2008). Smed-β-catenin-1 is required for anteroposterior
544 blastema polarity in planarian regeneration. *Science*, *319*(5861), 327–330.
545 https://doi.org/10.1126/science.1149943
546 Prud'homme, B., Lartillot, N., Balavoine, G., Adoutte, A., & Vervoort, M. (2002). Phylogenetic
547 analysis of the Wnt gene family: insights from lophotrochozoan members, *12*(16), 1395–
548 1400.
549 Sureda-Gómez, M., Martín-Durán, J. M., & Adell, T. (2016). Localization of planarian β-CATENIN-
550 1 reveals multiple roles during anterior-posterior regeneration and organogenesis.
551 *Development*, *143*(22), 4149–4160. https://doi.org/10.1242/dev.135152
552 Tanaka, E. M., & Reddien, P. W. (2011). The cellular basis for animal regeneration.
553 *Devlopmental Cell*, *21*(1), 172–185. https://doi.org/10.1016/j.devcel.2011.06.016
554 Tanaka, E., & Weidinger, G. (2008). Heads or tails: can Wnt tell which one is up? *Nature Cell*
555 *Biology*, *10*(2), 122–124. https://doi.org/10.1038/ncb0208-122
556 Thisse, C., & Thisse, B. (2008). High-resolution in situ hybridization to whole-mount zebrafish
557 embryos. *Nature Protocols*, *3*(1), 59–69. https://doi.org/10.1038/nprot.2007.514
558 Yokoyama, H., Ogino, H., Stoick-Cooper, C. L., Grainger, R. M., & Moon, R. T. (2007). Wnt/beta-
559 catenin signaling has an essential role in the initiation of limb regeneration. *Developmental*
560 *Biology*, *306*(1), 170–178.

561 Yoshida-Noro, C., & Tochinai, S. (2010). Stem cell system in asexual and sexual reproduction of
562 Enchytraeus japonensis (Oligochaeta, Annelida). *Development, Groth & Differentiation*,
563 *52*(1), 43–55. https://doi.org/10.1111/j.1440-169X.2009.01149.x
564 Zattara, E. E., Turlington, K. W., & Bely, A. E. (2016). Long-term time-lapse live imaging reveals
565 extensive cell migration during annelid regeneration. *BMC Developmental Biology*, *16*(6).
566 https://doi.org/10.1186/s12861-016-0104-2.
567 Zheng, P., Shao, Q., Diao, X., Li, Z., & Han, Q. (2016). Expression of stem cell pluripotency factors
568 during regeneration in the earthworm Eisenia foetida. *Gene*, *575*(1), 58–65.
569 https://doi.org/10.1016/j.gene.2015.08.034.
570 Zrzavý, J., Říha, P., Piálek, L., & Janouškovec, J. (2009). Phylogeny of Annelida (Lophotrochozoa):
571 Total-evidence analysis of morphology and six genes. *BMC Evolutionary Biology*, *9*(1), 1–14.
572 https://doi.org/10.1186/1471-2148-9-189
573

Figures

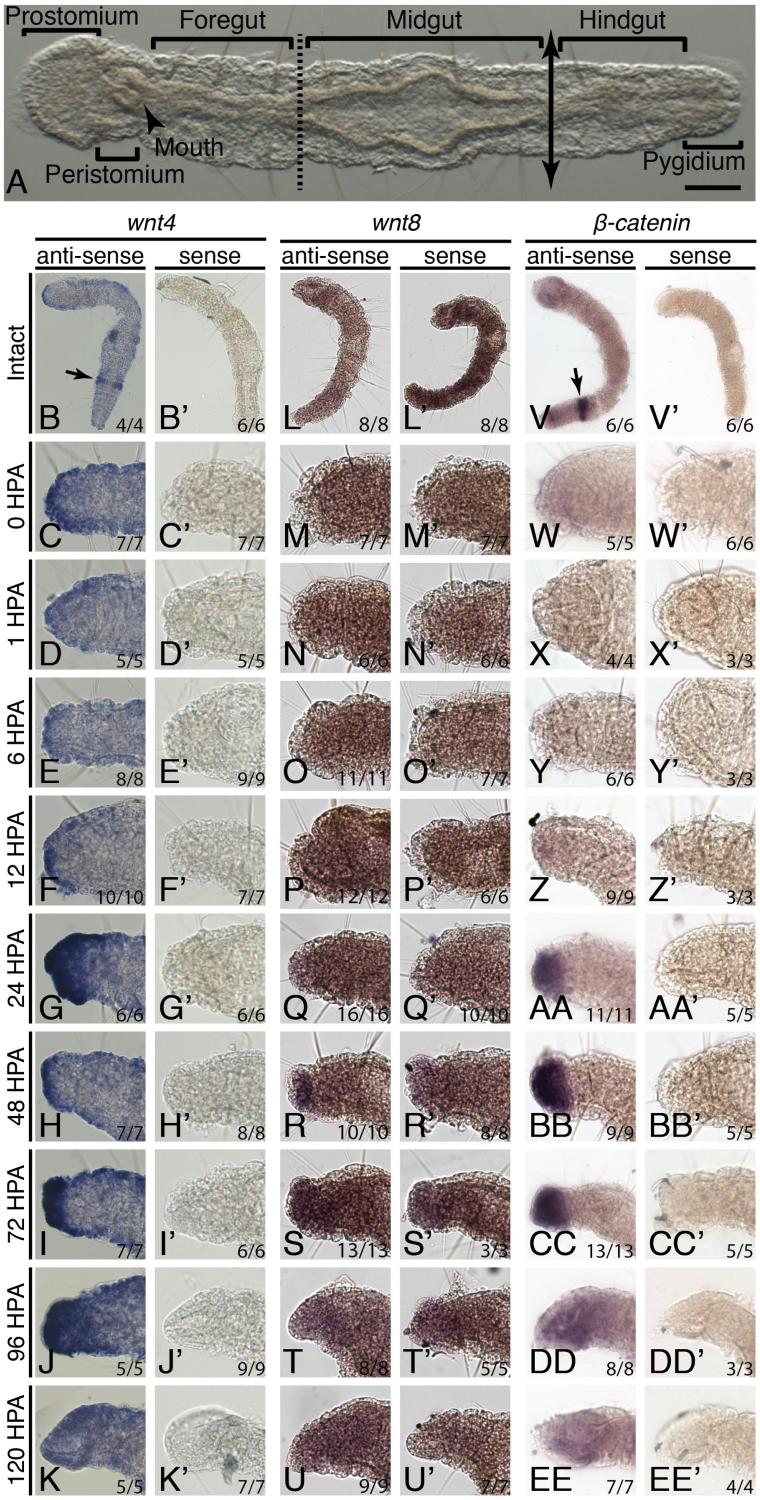
Prostomium
Foregut
Midgut
Hindgut
Mouth
Peristomium
Pygidium
A
wnt4
wnt8
β-catenin
anti-sense
sense
anti-sense
sense
anti-sense
sense
Intact
0 HPA
1 HPA
6 HPA
12 HPA
24 HPA
48 HPA
72 HPA
96 HPA
120 HPA
B 4/4
B' 6/6
L 8/8
L' 8/8
V 6/6
V' 6/6
C 7/7
C' 7/7
M 7/7
M' 7/7
W 5/5
W' 6/6
D 5/5
D' 5/5
N 6/6
N' 6/6
X 4/4
X' 3/3
E 8/8
E' 9/9
O 11/11
O' 7/7
Y 6/6
Y' 3/3
F 10/10
F' 7/7
P 12/12
P' 6/6
Z 9/9
Z' 3/3
G 6/6
G' 6/6
Q 16/16
Q' 10/10
AA 11/11
AA' 5/5
H 7/7
H' 8/8
R 10/10
R' 8/8
BB 9/9
BB' 5/5
I 7/7
I' 6/6
S 13/13
S' 3/3
CC 13/13
CC' 5/5
J 5/5
J' 9/9
T 8/8
T' 5/5
DD 8/8
DD' 3/3
K 5/5
K' 7/7
U 9/9
U' 7/7
EE 7/7
EE' 4/4

577 **Fig. 1. Regenerating wounds show *wnt4* and *β-catenin* activation during blastemal cell**
578 **proliferation.** (**A**) Dorsal view of an intact worm. Double arrow line indicates posterior
579 synchronizing cutting plane between midgut and hindgut junction. Dotted line indicates the
580 anterior amputation plane between foregut and midgut junction. (**C**-**K'**) *wnt4* expression
581 pattern during regeneration. Epithelial *wnt4* signal decreased within the first 6 HPA (**C**-**E**),
582 followed by activation in the blastema between 24-96 HPA (**G**-**J**). (**M**-**U'**) *wnt8* expression in the
583 blastema was indistinguishable from background signals. (**W**-**EE'**) *β-catenin* expression pattern
584 during regeneration. *β-catenin* was activated in the blastema between 24-72 HPA (**AA**-**CC**). In
585 intact worms, *wnt4* and *β-catenin* could be detected at the posterior proliferating segments of
586 intact worms (arrows of **B** and **V**). Ratio at the lower right corner indicates specimens showing
587 the corresponding expression patterns. Scale bar in **A** = 100 µm.
588

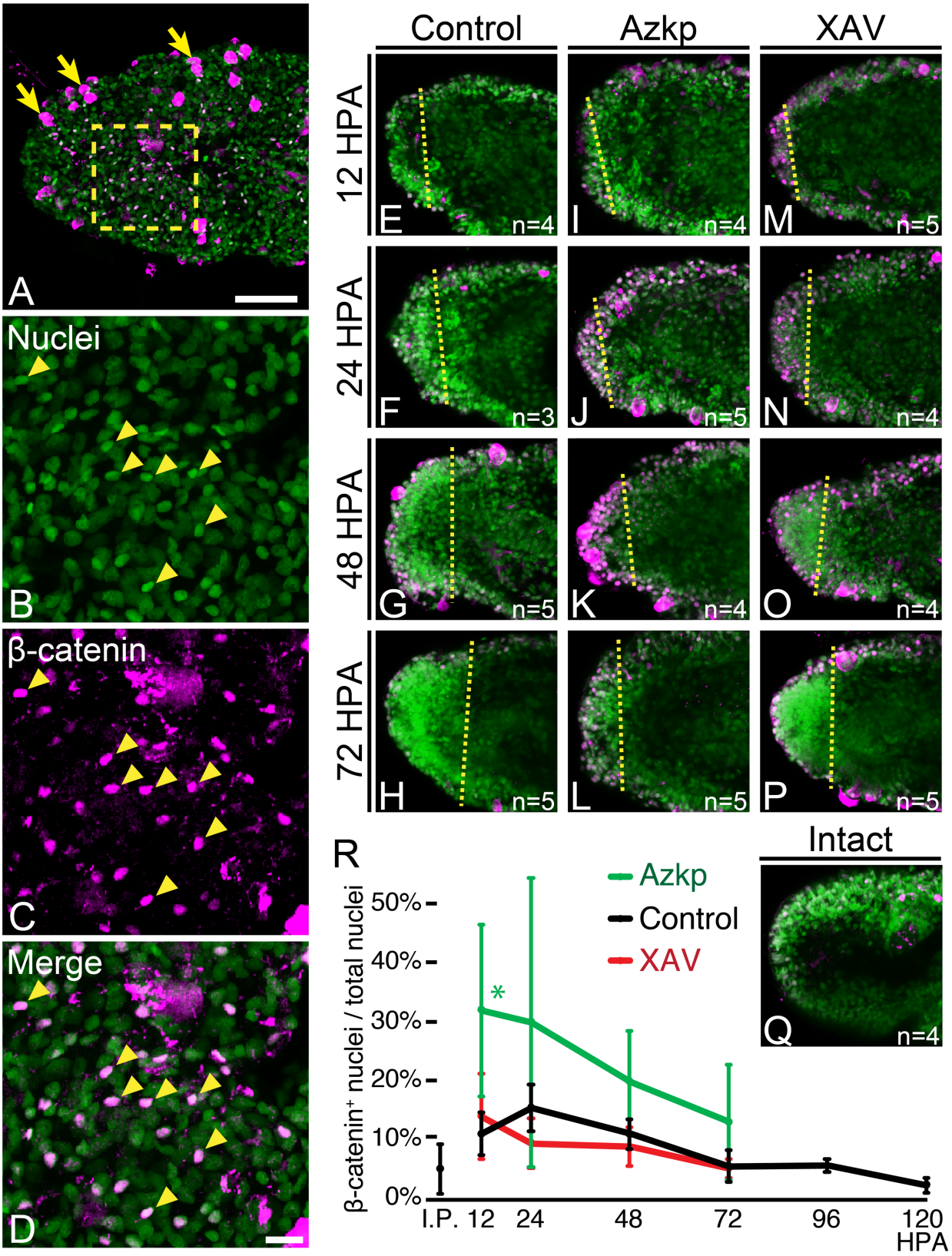
A
Nuclei
B
β-catenin
C
Merge
D
Control
Azkp
XAV
12 HPA
24 HPA
48 HPA
72 HPA
E
n=4
I
n=4
M
n=5
F
n=3
J
n=5
N
n=4
G
n=5
K
n=4
O
n=4
H
n=5
L
n=5
P
n=5
R
Azkp
Control
XAV
β-catenin+ nuclei / total nuclei
50%
40%
30%
20%
10%
0%
*
I.P.
12
24
48
72
96
120
HPA
Intact
Q
n=4

589

590 **Fig. 2. Nuclear β-catenin suggests Wnt pathway activation during blastemal proliferation at**
591 **24 HPA.** (**A**-**D**) Ventral view of 24 HPA blastema shows β-catenin protein (*magenta*)
592 accumulated in some nuclei (*green*) as indicated by arrowheads. Some non-specific signals were
593 also detected on the epithelium (arrows). (**B**-**D**) Higher magnification of the box region in **A**. (**E**-
594 **P**) Representative images of nuclear β-catenin at regeneration stages under control or inhibitor
595 treatments. (**Q**) Intact prostomium of β-catenin immunohistochemistry stain. (**R**) The ratio of β-
596 catenin^{+} nuclei to total blastemal nuclei under different conditions. Control blastema showed
597 highest level of β-catenin^{+} at 24 HPA. Azkp enhanced nuclear β-catenin level (*green* line), while
598 XAV down-regulated nuclear β-catenin level at 24 and 48 HPA (*red* line). **E**-**Q** are maximum
599 projections from ten serial focal planes. Error bars represent the standard deviation of the
600 mean from >3 worms. I.P. = Intact prostomium. Scale bar of **C** = 100 µm; **C'** = 10 µm. *Yellow*
601 dotted lines of **E**-**P** indicate the amputation plane. * denotes $p<0.05$ of *t*-test compared with
602 control at the corresponding time point.
603

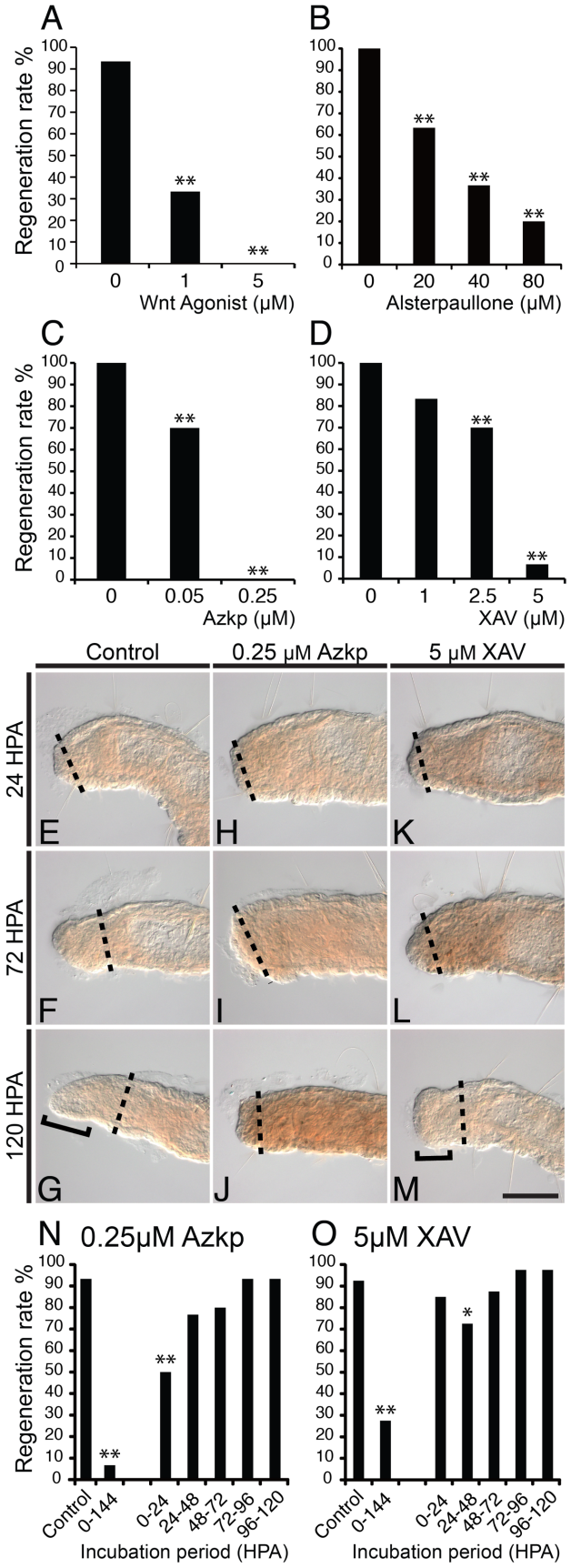
A
B
C
D
Regeneration rate %
Wnt Agonist (μM)
Alsterpaullone (μM)
Azkp (μM)
XAV (μM)
Control
0.25 μM Azkp
5 μM XAV
24 HPA
72 HPA
120 HPA
E
F
G
H
I
J
K
L
M
N 0.25μM Azkp
O 5μM XAV
Control
0-144
0-24
24-48
48-72
72-96
96-120
Incubation period (HPA)

604

605 **Fig. 3. Over-activating and down-regulating Wnt pathway both inhibited regeneration.** (**A**-**D**)
606 Exogenous Wnt pathway activators (Wnt agonist, Alsterpaullone and Azakenpaullone), and
607 inhibitor (XAV939), inhibited regeneration in dose-dependent manners. (**E**-**M**) Lateral view of
608 regeneration stages under control, 0.25 µM Azkp or 5 µM XAV treatments. Azkp treated worms
609 showed smaller blastema (**H**-**J**). XAV939 did not affect blastema formation (**K**-**M**), but worms did
610 not regenerate prostomium (compare bracket regions of **G** and **M**). (**N**-**O**) Successful
611 regeneration rates under 24H pulses. Regeneration was significantly inhibited by 0.25 µM Azkp
612 treatment between 0-24 HPA (**N**), and by 5 µM XAV treatment between 24-48 HPA XAV (**O**).
613 Anterior end is toward the left and dorsal to the top. Dotted lines indicate cutting planes. Scale
614 bar in **M** = 100 µm. All images are at the same scale. * denotes $p<0.05$. ** denotes $p<0.01$.
615

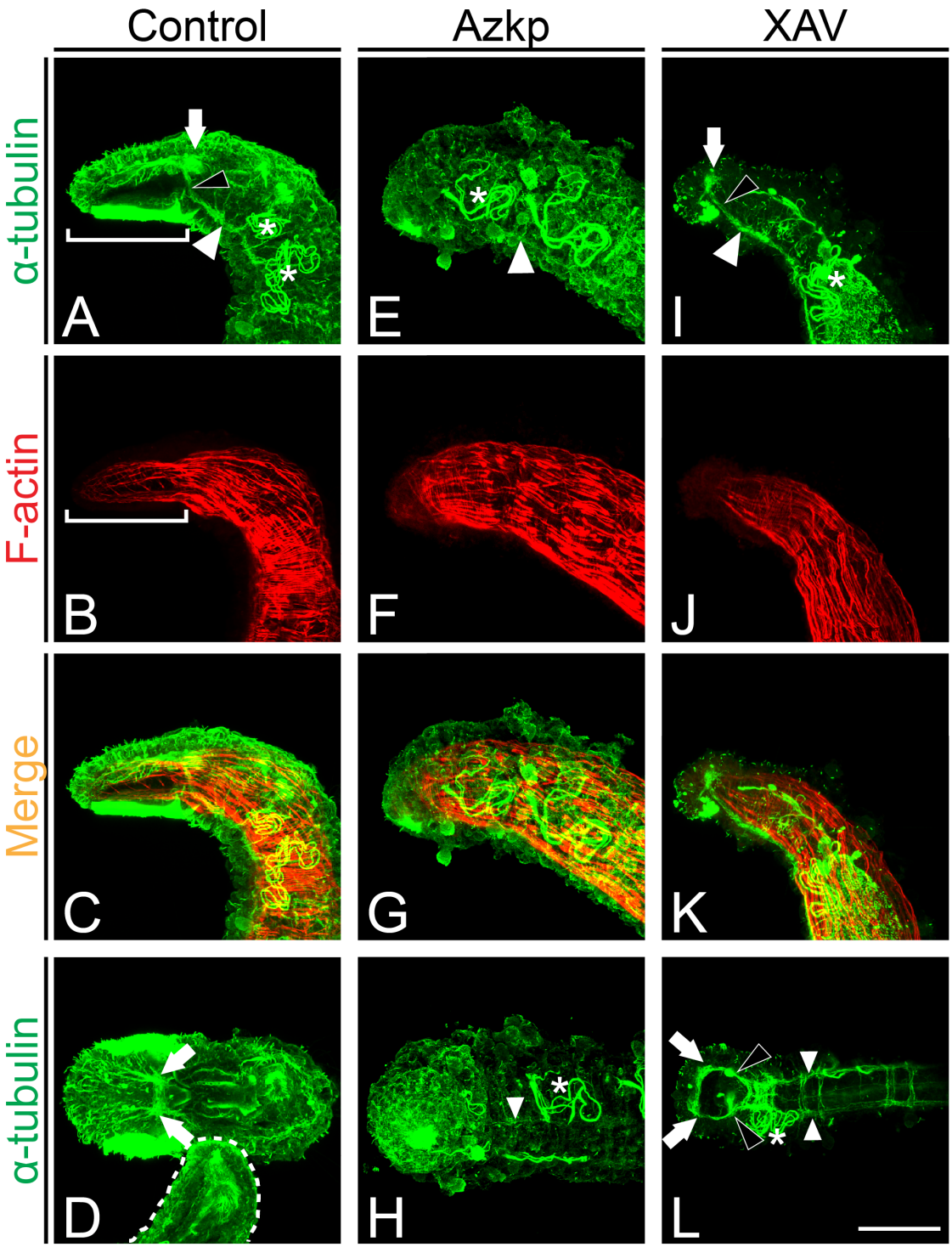

616
617 **Fig. 4. Over-activating Wnt pathway inhibited neuron regeneration and maintenance.** (**A-D**)

618 By 144 HPA, control worms showed recovered innervation (acetylated α-tubulin, *green*) with

619 neuropil in the prostomium (*white* arrows) connecting to the ventral nerve cord (*white*

620 arrowhead) by the circumesophageal commissures (*black* arrowhead). The neuropil extended
621 exons dorsal-anteriorly to the epithelial sensory cilia. Ventral prostomial ciliary field was also
622 enriched with acetylated α-tubulin (bracket of **A**). Rhomboid shape-arrayed muscle net (F-actin,
623 *red*) supported the flat prostomium (bracket region of **B**). The *white* dotted line in **D** delineates
624 the pygidium of the worm. (**E**-**H**) Azkp treated worms did not regenerate anterior innervations
625 from the degenerated ventral nerve cord (*white* arrowheads) and the prostomium (**F**). (**I**-**L**) XAV
626 treated worms regenerated anterior innervation where the neuropil (*white* arrows) and
627 circumesophageal commissures (*black* arrowheads) connect to the ventral nerve cords (*white*
628 arrowheads). However, these worms did not regenerate the prostomium (**J**). Asterisks indicate
629 metanephridia. Anterior of all amputees are toward the left. Figure **A**-**C**, **E**-**G**, and **I**-**K** are lateral
630 views with dorsal to the top. Figure **D** is dorsal view; **H** and **L** are ventral views. Scale bar in **L**
631 =100 µm. All images are at the same scale.
632

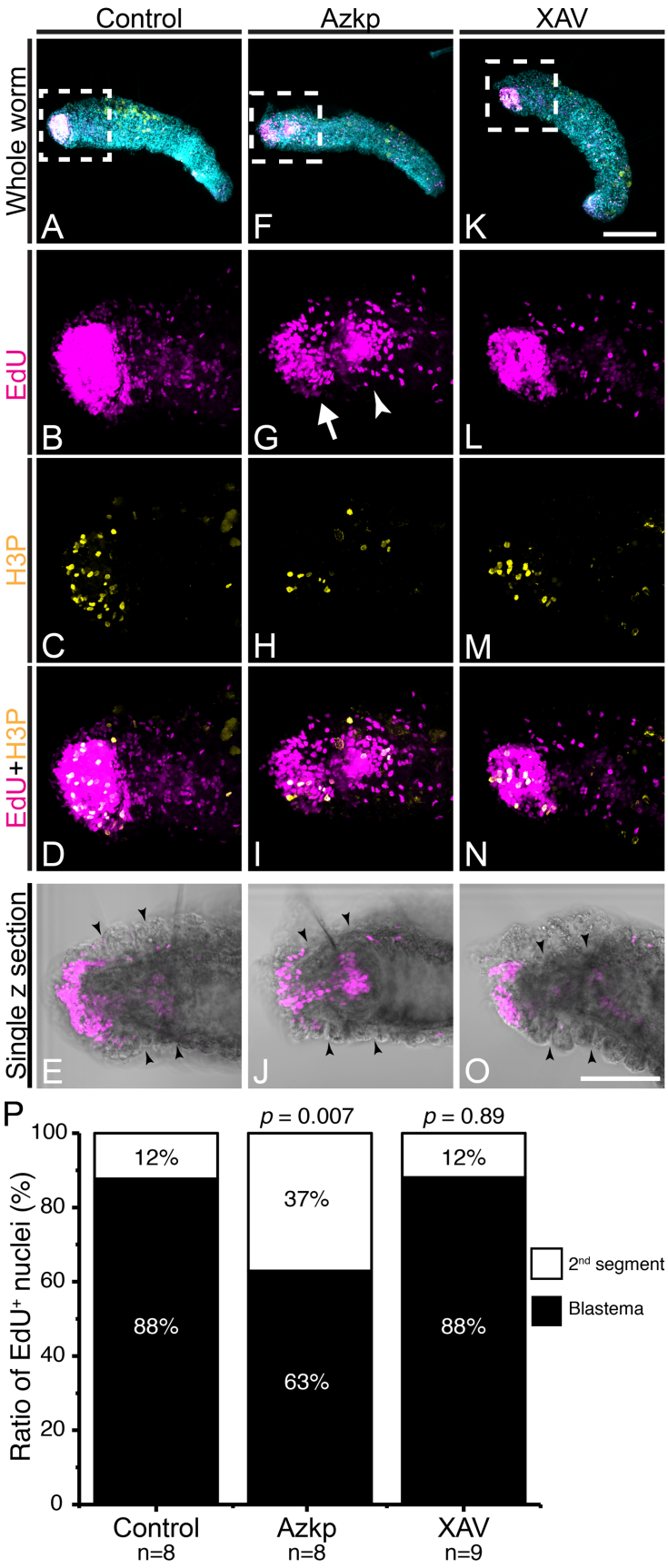
Control
Azkp
XAV
Whole worm
EdU
H3P
EdU+H3P
Single z section
A
B
C
D
E
F
G
H
I
J
K
L
M
N
O
P
p = 0.007
p = 0.89
Ratio of EdU+ nuclei (%)
100
80
60
40
20
0
12%
88%
37%
63%
12%
88%
2nd segment
Blastema
Control
n=8
Azkp
n=8
XAV
n=9

633

634 **Fig. 5. Over-activating Wnt pathway impaired blastemal cell proliferation.** (**A**-**O**) Proliferating
635 cells between 24 to 48 HPA are labeled by EdU (*magenta*) or anti-H3P antibody (*yellow*). The
636 nuclei are false-colored in *cyan*. Higher magnification views of *white* rectangle areas of **A**, **F** and
637 **K** are in the corresponding lower panels. In control and XAV treated worms, active proliferating
638 blastema showed condensed EdU signals (**B** and **L**); while Azkp treatment resulted in less EdU^+
639 nuclei at the wound site (arrow) and a second domain of proliferating cells in the 2nd segment
640 (arrowhead, **G**). (**J**) Single z section image shows that the proliferating cells in the 2nd segment
641 were located at the front end of midgut. Anterior of all amputees are toward the left with
642 dorsal to the top. Black arrowheads in **E**, **J** and **O** delineate the blastema and the segment
643 boundary. (**P**) Ratio of EdU^+ nuclei between blastema and the following 2nd segment. Student *t*-
644 test comparison with control worms shows significant ($p = 0.007$) enrichment of EdU^+ nuclei at
645 the 2nd segment of Azkp treated blastema. Scale bar in **K** = 200 µm; **O** = 100 µm. **A**, **F** and **K** are
646 at the same scale. **B-E**, **G-J** and **L-O** are at the same scale.
647

648

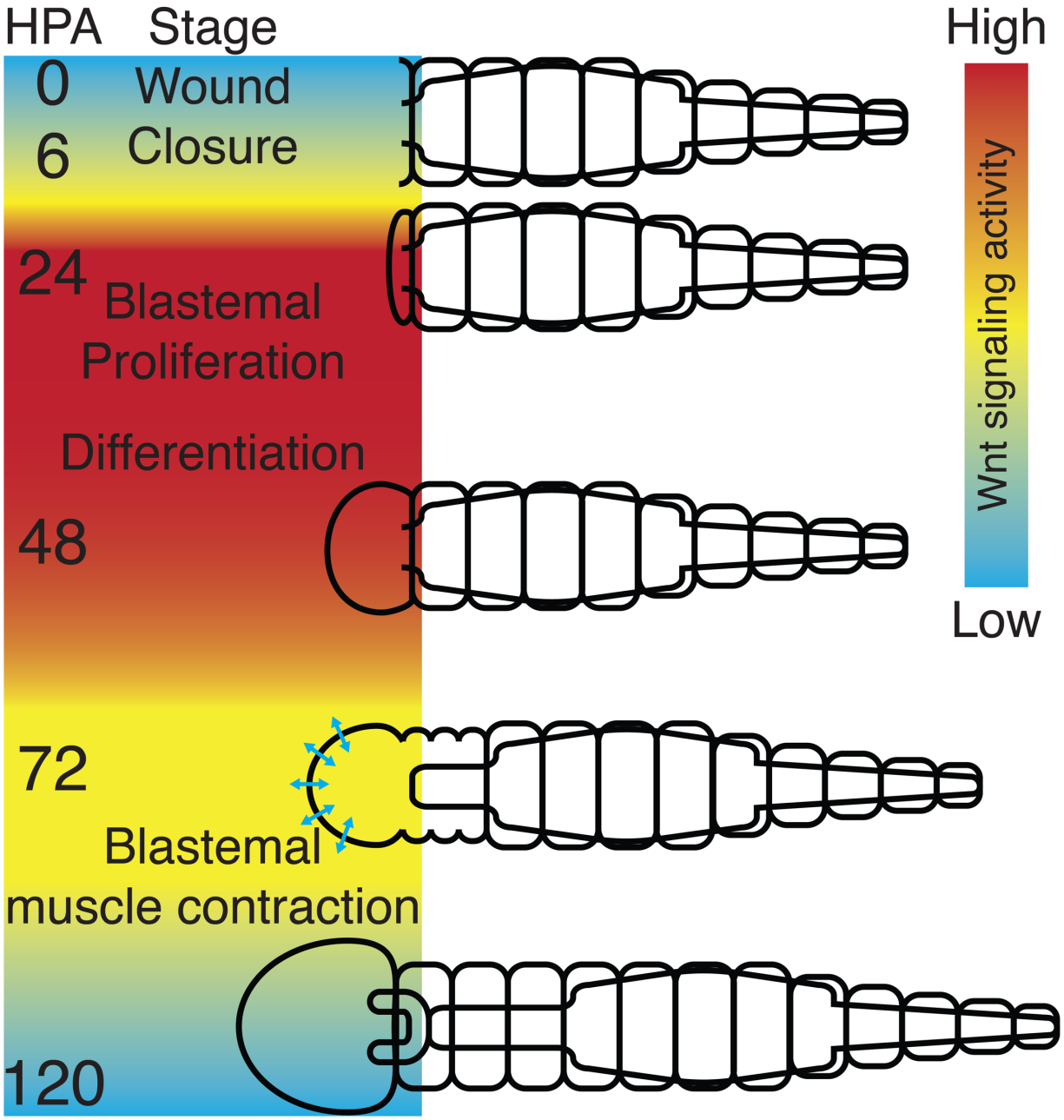

649

650 **Fig. 6. A proposed model of endogenous Wnt pathway activity during *A. viride* regeneration**.

651 A rainbow pallet defines hypothesized blastemal Wnt activities. After amputation, wound

652 closure finishes in the first 6 HPA. Then blastema gradually enlarges at the wound site by cell

653 proliferation. By 72 HPA, blastemal tissue initiates occasional contraction, indicating neuron

654 and muscle cell differentiation. By 120 HPA, worms complete regeneration with a horseshoe-

655 shaped mouth and can freely glide on substrates.

656

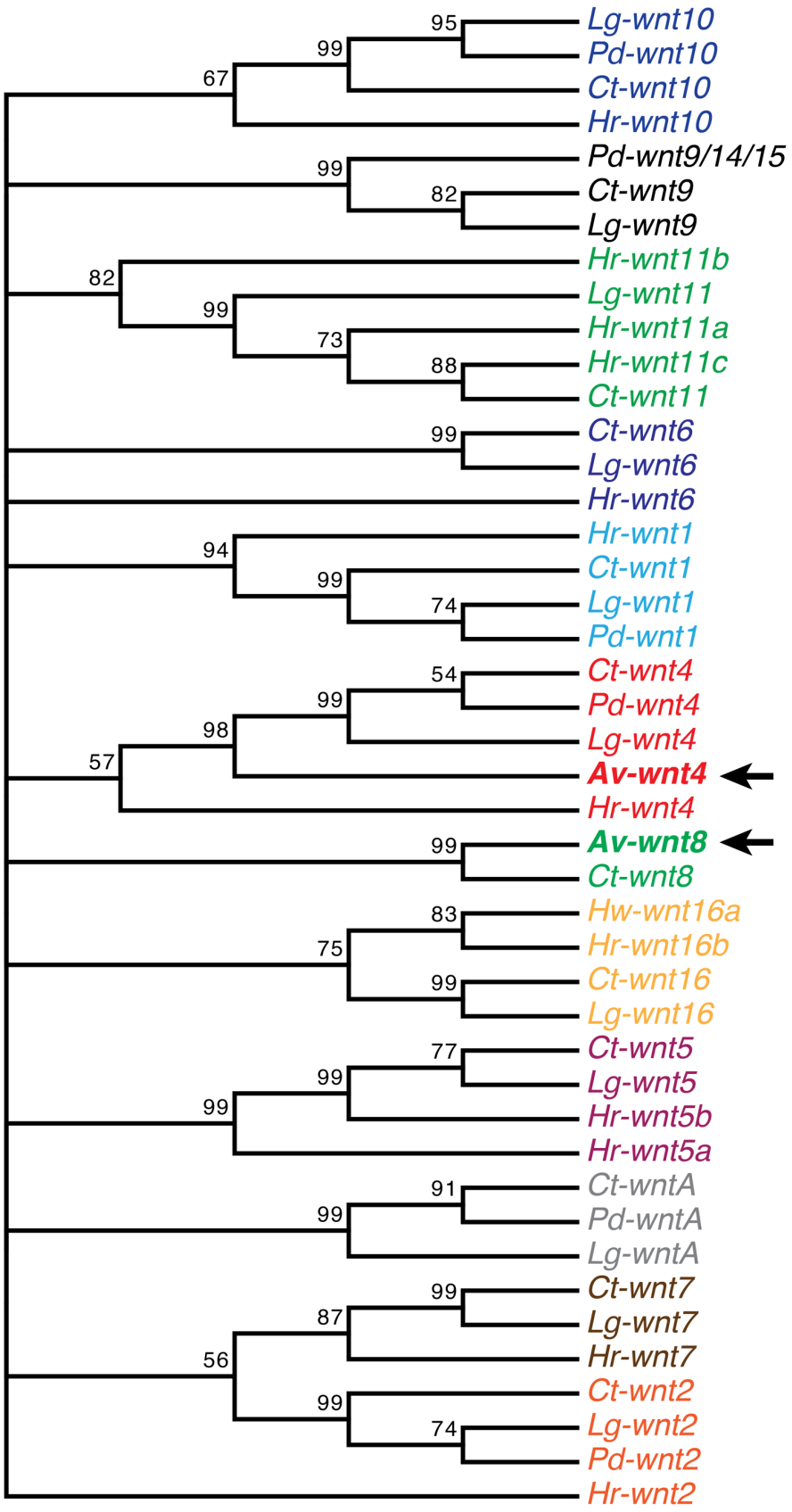
Lg-wnt10
Pd-wnt10
Ct-wnt10
Hr-wnt10
Pd-wnt9/14/15
Ct-wnt9
Lg-wnt9
Hr-wnt11b
Lg-wnt11
Hr-wnt11a
Hr-wnt11c
Ct-wnt11
Ct-wnt6
Lg-wnt6
Hr-wnt6
Hr-wnt1
Ct-wnt1
Lg-wnt1
Pd-wnt1
Ct-wnt4
Pd-wnt4
Lg-wnt4
Av-wnt4
Hr-wnt4
Av-wnt8
Ct-wnt8
Hw-wnt16a
Hr-wnt16b
Ct-wnt16
Lg-wnt16
Ct-wnt5
Lg-wnt5
Hr-wnt5b
Hr-wnt5a
Ct-wntA
Pd-wntA
Lg-wntA
Ct-wnt7
Lg-wnt7
Hr-wnt7
Ct-wnt2
Lg-wnt2
Pd-wnt2
Hr-wnt2
95
99
67
99
82
82
99
73
88
99
94
99
74
54
99
98
57
99
83
75
99
77
99
99
91
99
99
87
56
99
74

657

658 **Fig. 7. Neighbor-joining tree clusters *A. viride wnt* genes into the corresponding**

659 **Lophotrochozoan *wnt* subfamilies.** *Av-wnt4* and *Av-wnt8* are indicated by arrows. Within the

660 10,000 replicates bootstrap tests, the percentage of replicate trees in which the associated taxa

661 clustered together are shown at the branches. Note that the nodes with bootstrap percentage

662 <50% are compressed. Species name abbreviations: *Av: Aeolosoma viride*; *Ct*: *Capitella teleta*;

663 *Hr*: *Helobdella robusta*; *Lg*: *Lottia gigantea*; *Pd*: *Platynereis dumerilii*.

664

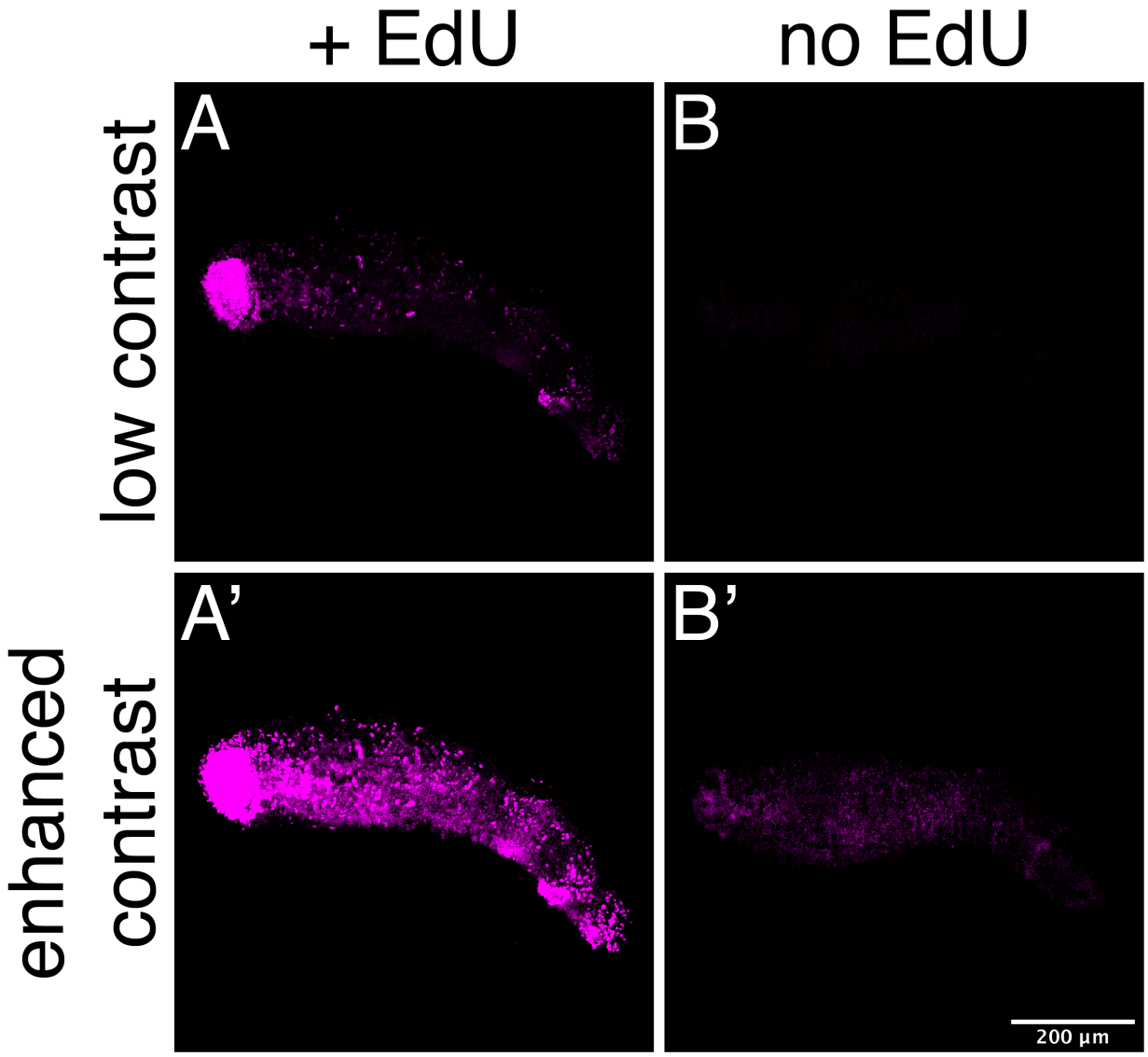

Fig. 8. EdU incubation specifically labeled proliferating cells. The regenerating worms were incubated with or without EdU between 24-48 HPA. Without EdU, background signal appeared only when the contrast of image was highly enhanced (**B'**).

671 **Table 1.** Degenerate primers initially used to clone Wnt pathway related genes.

Primer name	Sequence
wnt4-F1	CCDCGYGGRCAGCAAAGCA
wnt4-R1	ARTGCAARTGTCATGGHGTG
β-catenin-F1	GTGCGHCTGGCYGGHGGRYTGCA
β-catenin-R1	CRGCYRTVTGTGCTCTTCGTC

672 Code: M = A or C; B = C, G, or T; R = A or G; Y = C or T; V = A, C, or G; H = A, C, or T.

673

674 **Table 2.** Primers for 5' and 3' RACE. Note that *wnt4*-R2 and *β-catenin*-R2 were used as gene
675 specific primers for first strand cDNA synthesis during reverse transcription of 5' RACE.

Primer name	Sequence	Primer partner	Amplification target
3' AP	GGCCACGCGTCGACTAGTACTTTTTT TTTTTTTTTTTTT		
3' AP head	GGCCACGCGTCGACTAGTAC		
5' AP	GGCCACGCGTCGACTAGTACGGGG GGGGGGGGGGGG		
5' AP head	GGCCACGCGTCGACTAGTAC		
wnt4-F2	TTCAAAGCGTTGGCACAAGACTGC	3' AP	*wnt4* cDNA and *wnt4* 3' RACE 1st nested PCR
wnt4-F3	TCAAGGCACACGTGACGTTCTACA	3' AP head	*wnt4* 3' RACE 2nd nested PCR
wnt4-R2	GGTGAAGGCACTAGGTACACTAG	5' AP	*wnt4* 5' RACE 1st nested PCR
wnt4-R3	TGTAGAACGTCACGT	5' AP head	*wnt4* 5' RACE 2nd nested PCR
wnt8-F1	GTGGACGAACACTGCGGCTGCA	3' AP	*wnt8* 3' RACE 1st nested PCR
wnt8-F2	GCGTTGCTCTCAGCCAACCGAA	3' AP head	*wnt8* 3' RACE 2nd nested PCR
β-catenin-F2	GATGCTGCTACTAAAGTGGATG	3' AP	*β-catenin* 3' RACE 1st nested PCR
β-catenin-F3	GCAAGAGGGTGCCACAGCTCC	3' AP	*β-catenin* 3' RACE 2nd nested PCR
β-catenin-F4	GACACCGTGGTACGACACGG	3' AP	*β-catenin* 3' RACE 3rd nested PCR
β-catenin-R2	GCCACCAGCTTCAACAACAGCAGG		*β-catenin* cDNA
β-catenin-R3	GTTCACCAGGACCTCCAGAAGCC	5' AP	*β-catenin* 5' RACE 1st nested PCR
β-catenin-R4	TAGCTTGCTTTCTTGGTTACC	5' AP head	*β-catenin* 5' RACE 2nd nested PCR

676

677 **Table 3.** Primers for synthesizing riboprobe templates.

Primer name	Sequence	Target product length (bp)
*wnt4*_ISH-F1	CATGTTGGAGAGCGCTGCC	792
*wnt4*_ISH-R1	CATGTGTATTCGTTGATGTGCAC	
*wnt8*_ISH-F1	CGGAGAGATGGTGAGTCGCCTT	934
*wnt8*_ISH-R1	TGTGCGGGCGTGCTTTGCGTAT	
*β-catenin*_ISH-F1	CGCAATGAAGGAGTTGCCAC	885
*β-catenin*_ISH-R1	TCGTCTACCATGTACACAGG	

678